Atomic and electronic structures of Ag/Si(111)-c(12×2) surface: A first-principles study

Feng-Chuan Chuang,[1,*] Chia-Hsiu Hsu,[1] Cai-Zhuang Wang,[2] and Kai-Ming Ho[2]
[1]*Department of Physics, National Sun Yat-Sen University, Kaohsiung 804, Taiwan*
[2]*Department of Physics and Astronomy, Iowa State University and Ames Laboratory, US Department of Energy, Ames, Iowa 50011, USA*
(Received 3 September 2008; revised manuscript received 31 October 2008; published 19 December 2008)

Structural models for the Ag/Si(111)-c(12×2) phase were identified from a systematic search using tight-binding molecular dynamics and first-principles total-energy calculations. Our calculations showed that the low-energy c(12×2) and 6×1 structures can be derived from the well-known honeycomb chain-channel 3×1 model. Two c(12×2) models are found to have lower surface energies than both the 3×1 and 6×1 models, which is consistent with the experimental observation. A distinct feature of the c(12×2) structure is the dimer formation induced by lateral displacements of Ag atoms within the same row in the 6×1 phase. Different packing patterns of the Ag dimers with the same surface area can lead to either 6×2 or c(12×2) phase with very similar energies. Simulated scanning tunneling microscope images from our c(12×2) structure are in excellent agreement with the experimental measurement. Moreover, the lowest-energy c(12×2) structure identified from our calculations also reproduces the key features in the angle-resolved photoemission measurement.

DOI: 10.1103/PhysRevB.78.245418 PACS number(s): 68.43.Bc, 68.35.B−

I. INTRODUCTION

The growth of metals on Si(111) surface has been the focus of many studies over the past several decades.[1] Two of the prototypical metal-semiconductor interfaces are the silver-silicon and gold-silicon interfaces. Considerable progress has been achieved in understanding the structures and properties of these two systems. One of these achievements is the determination of the Ag coverage on the 3×1 phase.[1–14] From a geometrical point of view, there are several possible Ag coverages (e.g., 1/3, 2/3, and 1 ML) and Si coverage (ranging from 1/3 to 2 ML in 1/3 ML increment) on a Ag/Si(111)-3×1 phase. In early experiments,[1–11] the 3×1 phase was observed by desorbing Ag from the Ag/Si(111)-$\sqrt{3}\times\sqrt{3}$ phase. Thus, exact amount of Ag and Si atoms desorbed from reconstruction are difficult to estimate. Two possible Ag coverages, 1/3 ML and 2/3 ML, for the 3×1 phase have been debated in the experiments.[1–10] It was not until recently that almost all experimental and theoretical studies pointed toward 1/3 ML as the most stable Ag coverage for the 3×1 phase.[12–14]

Despite these advances, many issues of the Ag/Si interface still remain unresolved. One of these problems is the phase transitions from the 3×1 to 6×1 and from 6×1 to c(12×2) on Ag/Si(111).[8,12,14–20] The 3×1 phase was observed after desorbing Ag atoms by annealing around $T>893$ K from the $\sqrt{3}\times\sqrt{3}$ phase. As the temperature was cooled down to around 400–500 K, it undergoes a phase transition from 3×1 to 6×1. Moreover, if the temperature is further decreased to around 100 K,[17,18] another phase transition from 6×1 to c(12×2) takes place. Based on the similarities of angle-resolved photoemission spectroscopy (ARPES) data from different phases, Sakamoto *et al.*[17] concluded that 6×1 and c(12×2) phases originated from the same honeycomb chain-channel (HCC) 3×1 model. Recently, a model for these phase transitions was proposed by Miyata *et al.*[18] based on their scanning tunneling microscope (STM) experiment and previous theoretical calculations.[14] It was suggested that the nature of the 3×1-to-6×1 and 6×1-to-c(12×2) phase transitions could be described as in-plane (horizontal) and out-of-plane (vertical) displacements of Ag atoms from the HCC model, respectively.[18] Furthermore, they concluded that the two-step transition seems to be the order-disorder type associated with two different types of the Ag adsorption sites. As a result, these two order-disorder phase transitions occur at different temperatures due to different heights of potential barriers between the equivalent stable atomic configurations.[18] However, this mechanism has not been rigorously investigated theoretically using first-principles calculations.

In this paper, we examine several previously proposed structural models and perform systematic searches for the lowest-energy models for 3×1, 6×1, and c(12×2) phases. Our searches are based on both HCC model of Ag/Si(111)-3×1 (Refs. 12–14) and the double honeycomb chain (DHC) model of Au-Si(111)-5×2.[21–24] The low-energy structural candidates selected from the combinatorial search using the tight-binding molecular dynamics[25,26] were further optimized using first-principles total-energy calculations. The extensive calculations showed that the previously proposed structural models, the HCC model and its variant, are indeed the lowest-energy models for the 3×1 and 6×1 phases, in both tight-binding and first-principles calculations. The 6×1 phase is derived from the HCC 3×1 phase in which the Ag atoms in the adjacent row are located in the two equivalent sites (β_T and β_T'). In order to obtain the structure for the c(12×2) phase, we use the same search technique as that in our previous study.[24] Unlike the mechanism proposed by Miyata *et al.*,[18] in our discovered structural models, the two Ag atoms in the 6×1 phase are moved horizontally which then form Ag dimers along the Ag rows to form either the 6×2 or the c(12×2) phases. The c(12×2) models from our calculations have lower energies than both the 3×1 and 6×1 phases. Through comparisons with the previous experimental STM images[18] and our simulated STM images, the final atomic structural model for the c(12×2) phase was obtained.

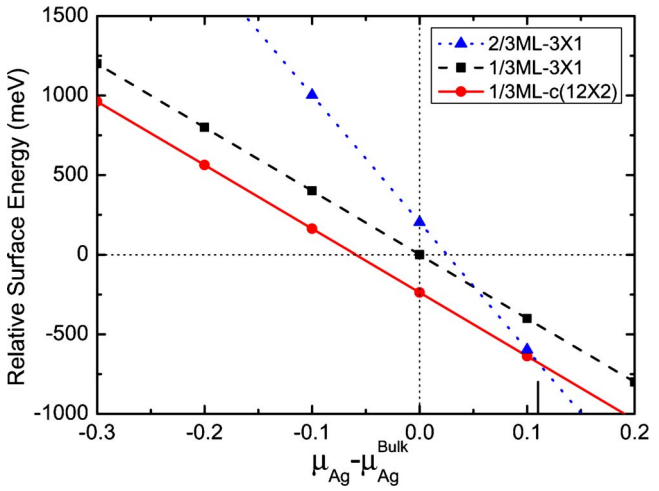

FIG. 1. (Color online) The relative surface energy as a function of the $\mu_{Ag}-\mu_{Ag}^{bulk}$ for the lowest-energy 1/3-ML 3×1 and c(12 $\times2$) structures as well as the lowest-energy 2/3-ML 3×1 structure.

II. COMPUTATIONAL METHODS

The first-principles calculations were carried out within the generalized gradient approximation as parametrized by Perdew, Burke, and Ernzerhof (PBE) (Ref. 27) to density-functional theory[28] using projector-augmented-wave (PAW) potentials,[29] as implemented in *Vienna ab initio Simulation Package* (VASP).[30] The reference configuration $4s^13d^{10}$ (to indicate valence electrons) is used for generating the Ag PAW potential. All the models considered here, except for the c(12$\times$2) models, were examined using a 6×2 supercell in order to have the same level of accuracy in k-point sampling. We further compare the total energies of the 3×1 and 6×1 structures using both the 6×2 and c(12$\times$2) supercells and found that the difference of using these two supercells is rather small and within 1 meV. Since the area of the 6×2 and c(12$\times$2) phases are the same, we shall use this as the basis for determining the surface energy in our present study. The kinetic-energy cutoff was set to 250 eV and the 2×4 Monkhorst-Pack grid was used to sample the surface Brillouin zone (BZ). Moreover, for all our surface calculations, the Si bulk lattice constant of 5.465 Å was used throughout. The Ag/Si(111) surface was modeled by a periodically repeating slab consisting of three Si bilayers, a reconstructed layer, and a vacuum gap of ~12 Å along the direction normal to the surface. Hydrogen atoms were used to passivate the Si dangling bonds at the bottom of the slab at a Si-H distance of 1.509 Å along the ideal crystalline directions while their positions were kept fixed. Similarly, the silicon atoms of the bottom bilayer were kept fixed at the bulk crystalline positions. The remaining Si and Au atoms were relaxed until the residual force was smaller than 0.01 eV/Å.

For the tight-binding calculations, the supercell used consists of three Si bilayers and a reconstructed layer. As in the VASP calculations, the silicon atoms of the bottom bilayer were kept fixed at the bulk crystalline positions. The remaining Si and Au atoms were relaxed via the steepest-descent method until the residual force was smaller than 0.01 eV/Å. The tight-binding parameters involving Si and Ag are summarized in Refs. 25 and 26. The computational details of the combinatorial search have been presented elsewhere[24] and will not be elaborated here.

TABLE I. The relative surface energies ΔE_s (meV per 6 $\times2$ unit cell) with respect to HCC-$\beta_T(3\times1)$ model using the 6 $\times2$ supercell.

Reconstruction	Model label	Figure	ΔE_s 6×2 cell	ΔE_s c(12$\times$2) cell
3×1	HCC-$T4$	2(a)	508.6	
	HCC-$H3$	2(a)	527.7	
	HCC-β_T or β_T'	2(b)	0.0	0.4
	2/3 ML	2(c)	203.3	
3×2	HCC dimer	2(d)	−94.1	
6×1	DHC-like	2(f)	875.6	
6×1	HCC-$\beta_T\beta_T'$	2(e)	−190.9	−190.2
6×2	DHC-like	2(g)	889.4	
6×2	HCC-β_T-β_T'-dimer n1	3(a)	−218.9	
6×2	HCC-β_T-β_T'-dimer n2	3(b)	−219.1	
c(12$\times$2)	HCC-β_T-β_T'-dimer n1	3(c)		−200.6
c(12$\times$2)	HCC-β_T-β_T'-dimer n2	3(d)		−237.3

Having computed the total energies of the models, the relative surface energy with respect to the HCC-$\beta_T3\times1$ structure using the 6×2 supercell, ΔE_s, is calculated according to the relation

$$\Delta E_s = E_{\text{model}} - E_{\text{HCC-}\beta_T} - \Delta N_{\text{Si}} \times \mu_{\text{Si}} - \Delta N_{\text{Ag}} \times \mu_{\text{Ag}}. \quad (1)$$

In the above, $E_{\text{HCC-}\beta_T}$ and E_{model} are the total energies of the reference HCC-$\beta_T(3\times1)$ structure and the structural model under investigation, respectively. ΔN_{Si} and ΔN_{Ag} are the differences in the number of the Si and Ag atoms with respect to the HCC-$\beta_T(3\times1)$ model. μ_{Si} represents the chemical potential of Si and is set to the bulk energy of Si. We have analyzed the stability of the different surface structures as a function of μ_{Ag}. The surface energies of the lowest-energy 3×1 and c(12$\times$2) structures at the Ag coverages of 1/3 ML as well as the lowest-energy 2/3 ML-3×1 model were plotted as a function of $\mu_{\text{Ag}}-\mu_{\text{Ag}}^{\text{bulk}}$ in Fig. 1, where $\mu_{\text{Ag}}^{\text{bulk}}$ is the bulk energy of the Ag. As can be seen in the plot, for $\mu_{\text{Ag}}-\mu_{\text{Ag}}^{\text{bulk}}<0.11$ eV, the surface energy of the 1/3-ML c(12 $\times2$) structure is lower than that of the 2/3-ML 3×1 structure. We note that the relative surface energy of the 2/3-ML 3×1 model listed in Table I is calculated by setting the bulk energy of Ag to the chemical potential of Ag in Eq. (1). For the models with both the same Ag and Si coverages, the relative surface energies will not depend on the choice of the chemical potentials of Ag and Si. All models considered here were calculated either using a 6×2 or c(12$\times$2) cell; thus the relative surface energies are evaluated based on the same surface area.

III. RESULTS AND DISCUSSION

Before constructing the structural model for the c(12 $\times2$) phase, we examine the structural models of the 3×1

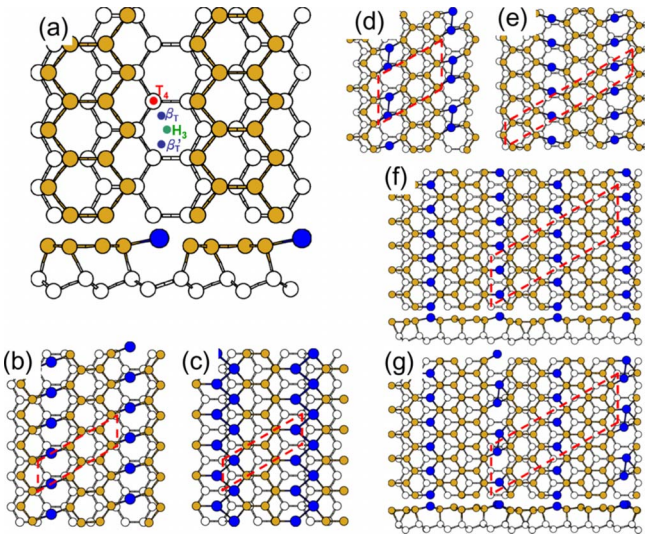

FIG. 2. (Color online) Structural models of the Ag/Si(111) systems. Silicon atoms at the reconstructed layer and at the upper part of the subsurface Si bilayer are marked in gold (light gray) and white, respectively. (a) The HCC model. The adsorption sites, $T4$, $H3$, β_T, and β_T', are labeled. (b) The lowest-energy structural models of the 3×1 phase, where the Ag atoms are all at either the β_T or β_T' sites. (c) The structural model for the 3×1 phase at Ag coverage of 2/3 ML obtained from Ref. 26. (d) The 3×2 model. The Ag atoms pair up to form dimers. (e) The 6×1 phase. (f) and (g) are the 6×1 and 6×2 models, respectively, and constructed in a manner similar to the double honeycomb chain models of Au/Si(111)-5×2.

phase at Ag coverage of 1/3 ML. The most widely accepted HCC model for the 3×1 phase is illustrated in Fig. 2(a). Here we adopt the same notation used by Miyata *et al.*[18] There are three possible adsorption sites in the HCC model and their energies from our calculations are summarized in Table I. Our first-principles calculations show that the Ag atom prefers to reside on either one of the two equivalent sites, namely, β_T or β_T', which are slightly away from the $T4$ site. The $T4$ and $H3$ sites have higher energies than the β_T and β_T'.

Although most of the models for the 3×1 phase from experimental and theoretical studies were based on the idea that the 3×1 phase is formed at Ag coverage of 1/3 ML, there are evidences suggesting that the 3×1 phase may also appear at Ag coverage of 2/3 ML.[8] Therefore, structural optimizations of the 3×1 phase were also performed at Ag coverage of 2/3 ML and at various Si coverages.[26] The lowest-energy model at Ag coverage of 2/3 ML as shown in Fig. 2(c) corresponds to Si coverage of 1 ML. The relative surface energy of this model (2/3 ML) using Eq. (1) is only 209 meV higher than the well-known HCC model (1/3 ML). However, when we attempted to construct the structure for the 6×1 phase based on this (2/3 ML) 3×1 model, we did not find any structure with lower energy than those of the 6×1 models derived from the (1/3 ML) HCC 3×1 structure. Therefore, for the rest of the study, we will solely focus on the HCC model with Ag coverage of 1/3 ML and search for the structures of the higher-order reconstruction phases [e.g., 6×1, 6×2, and c(12×2)] that has Ag coverage of 1/3 ML.

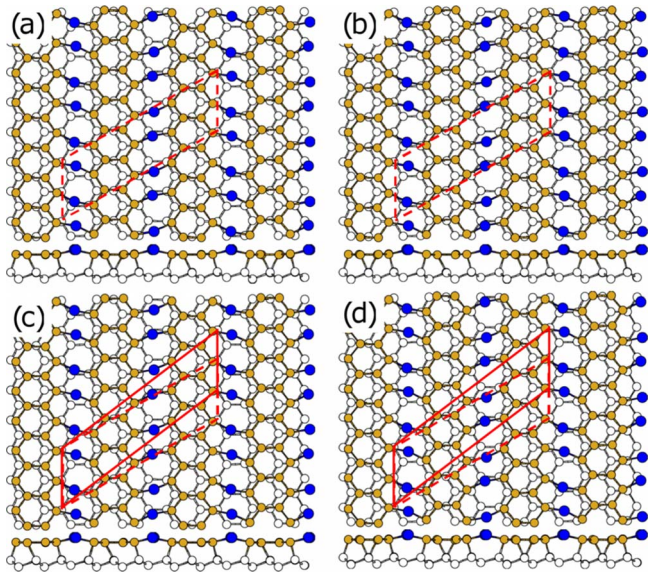

FIG. 3. (Color online) (a) and (b) are the 6×2 models. (c) and (d) are the c(12×2) models. The 6×2 cell is outlined with the dash lines, while the c(12×2) cell is outlined with the solid lines.

The structural model for the 6×1 phase has been previously proposed based on the HCC 3×1 model[12–14,17,18] simply by alternately varying the Si-Ag-Si bond configurations (β_T and β_T') between the adjacent rows as shown in Fig. 2(e). We found that the 6×1 model has a lower surface energy than the HCC 3×1 model by ~191 meV. In addition to the HCC-like model, the 6×1 phase can also be constructed in a similar manner to the DHC model of Au/Si(111)-5×2.[21–24] A combinatorial search[24] using tight-binding potential was implemented to search for the lowest-energy configuration of the Ag atoms on the 6×1 surface based on both HCC and DHC motifs. Low-energy candidates selected from the combinatorial search coupled with tight-binding calculations were further optimized using first-principles calculations. Unfortunately, our combinatorial searches did not uncover any other model that has a lower energy than the aforementioned HCC-β_T-β_T'6$\times$1 structure. Here we show the lowest-energy honeycomb (DHC-like) model for 6×1 from our search in Fig. 2(f). This DHC-like 6×1 model [Fig. 2(f)] was found to be 1066 meV higher than the energy of the lowest-energy HCC 6×1 model [Fig. 2(e)].

We also consider the structural model for the 6×2 phase using the combinatorial assignments of Ag and surface Si atoms within the 6×2 unit cell based on the HCC-like and DHC-like motifs. Similar to the case of 5×1 to 5×2 on Au/Si(111) in our previous study,[24] instead of the 45 and 55 models for 6×1, there are additional 2420 and 3630 models for 6×2 generated from HCC-like and DHC-like models to be optimized, respectively.[24,31] Low-energy candidates from tight-binding calculations were also selected for further optimization using first-principles calculations. However, this procedure does not reveal any 6×2 structure that has an energy lower than the known HCC 6×1 model shown in Fig. 2(e).

We note from our previous study of Au/Si(111)-5×2 that pairing up of Au atoms in the Au row leads to a more

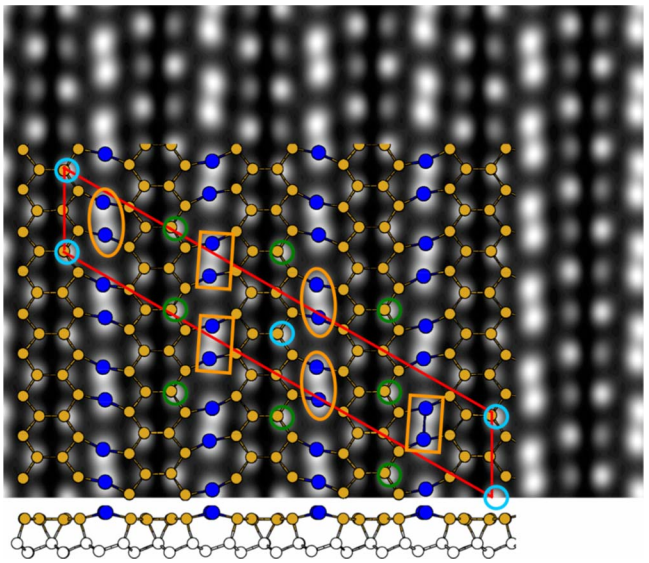

FIG. 4. (Color online) Simulated empty-state STM image with a sample bias of 2.0 V and atomic structure of the c(12×2) phase. The 12×2 cell is outlined with the solid lines. The circles, rectangles, and ovals in the figure are used to highlight the prominent features of experimental STM image as shown in Fig. 3(b) in Ref. 18.

stable structure.[24] By shifting the Ag metal atoms in the 3×1 and 6×1 phases closer together to allow dimerization along the metal rows, we found that the resulting one 3×2 and two 6×2 structures with Ag dimerization along the Ag rows as shown in Figs. 2(d), 3(a), and 3(b), respectively, have energy lower than the 3×1 [Fig. 2(b)] and 6×1 [Fig. 2(e)] structures. This indicates that the dimerization mechanism can further lower the energy. However, we also note that the dimerization of the Ag row on the Si(111) surface does not spontaneously take place when the optimization using the first-principles calculation at zero temperature was performed on the HCC 6×1 structure as discussed in the previous paragraph. This suggests that there is an energy barrier for the dimerization of the Ag rows.

Based on the dimerization mechanism, we can search for the structures of 6×2, c(12×2), and 12×2 simultaneously by enumerating all possible Ag dimers' relative positions within a 12×2 cell. All in all, there should be 16 possible structures. However, when translational symmetry is taken into account, only two 6×2 [see Figs. 3(a) and 3(b)], two c(12×2) [see Figs. 3(c) and 3(d)], and two 12×2 structures are distinct. The two 6×2 structures are found to be degenerate in energy. We also note that the two c(12×2) structures in Figs. 3(c) and 3(d) can be obtained by simply changing the surface unit vectors of two 6×2 structures in Figs. 3(a) and 3(b). Our calculations show that the c(12×2) model as shown in Fig. 3(d) has the lowest energy among all the models considered here. Also, the energy of the c(12×2) structure is lower than that of the 6×2 phase as can be seen in Table I. The energy ordering (from high to low) of 3×1 [Fig. 2(b)], 6×1 [Fig. 2(e)], and c(12×2) [Fig. 3(d)] models is consistent with the conception of a sequence of two order-disorder transitions.[8,12,14–18] In addition, we notice that these Ag dimers are not perfectly parallel to the $[11\bar{2}]$ direction

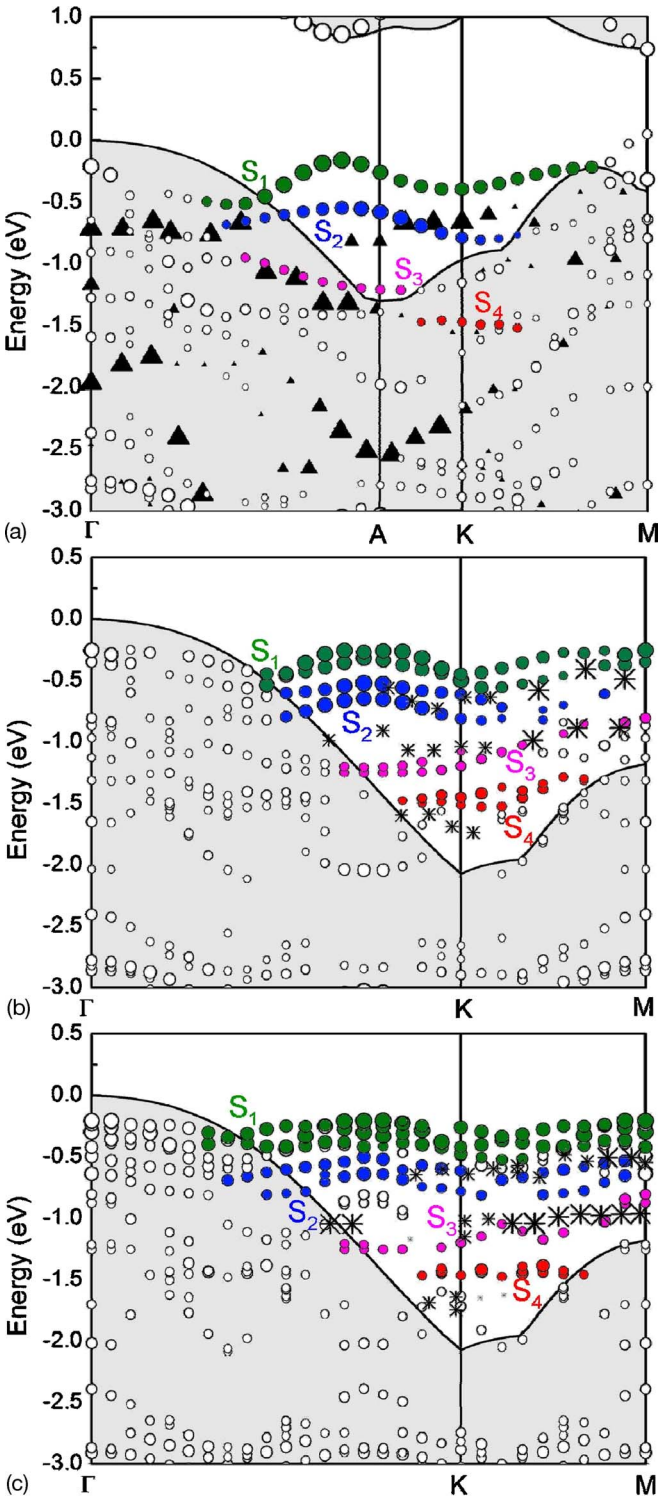

FIG. 5. (Color online) The band structures of the HCC (a) 3×1 [Fig. 2(b)], (b) 6×1 [Fig. 2(e)], and (c) c(12×2) [Fig. 3(d)] models. The projected bulk bands using (a) 3×1 and [(b) and (c)] 1×1 units are shaded. Filled triangles in (a) represent the ARPES data of Gurnett *et al.* (Ref. 16), which were uniformly shifted by 0.48 eV in order to line up with the projected bulk valence-band maxima from the calculations and thus for the easier comparison. The stars in (b) and (c) indicate three surface bands obtained from ARPES data of Sakamoto *et al.* (Ref. 17), which were uniformly shifted by 0.61 eV.

and instead tilted at an angle of $4.8 \pm 1°$. This small tilt may not be easy to resolve in the experiments. Furthermore, we note that the energy differences between the 6×2 and c(12 $\times2$) models are rather small except for the c(12×2) model shown in Fig. 3(d). We further calculated simulated STM images[32] for these four models (two for 6×2 phases and another two for c(12×2) phases). Focusing exclusively on the bright spots along the metal rows, we notice that these four models have similar STM images but with different dimer locations. Our simulated STM images show that small tilt of Ag dimers with respect to the $[11\bar{2}]$ direction is in agreement with the experimental STM images [see Fig. 3(b) in Ref. 18]. However, when further examining the less bright spots from the Si atoms within the honeycomb part, only the simulated STM image of the lowest-energy structure [shown in Figs. 3(d) and 4] is in excellent agreement with the experimental STM image [see Fig. 3(b) in Ref. 18]. Note that the simulated empty-state STM image at sample bias of 2.0 V for the c(12×2) structure is shown in Fig. 4.

Before discussing the band structure of the c(12×2) model, we first examine the band structures of the 3×1 [Fig. 2(b)] model. This model exhibits three major filled surface states (S_1, S_2, and S_3).[14] Filled triangles represent the ARPES data of Gurnett *et al.*,[16] which were uniformly shifted by 0.48 eV in order to line up with the projected bulk valence-band maxima from the calculations and thus for the easier comparison. The filled state band dispersions (S_2 and S_3) and relative positions from our calculations compare well with the ARPES data on Ag/Si(111)-(3×1),[16] whereas the S_1 seems invisible in the experiment.

The band structures of the HCC 6×1 [Fig. 2(e)] and c(12×2) [Fig. 3(d)] models are plotted in Figs. 5(b) and 5(c). These band structures are very similar to that of the 3 $\times1$ model. In the plot, we identified similar surface bands which are also found in the 3×1 model. The stars in Figs. 5(b) and 5(c) represent three surface bands obtained from the ARPES data of Sakamoto *et al.*[17] and uniformly shifted by 0.61 eV for easier comparison. As in the 3×1 case, the S_2, S_3, and S_4 bands compare reasonably well with the experimental data.[17]

Finally, we also examine the vertical displacement model for the 6×1 to c(12×2) transition proposed by Miyata *et al.*[18] To do this, we simply raise and lower the heights of the Ag atoms alternately at the β_T and β_T' sites to obtain the 3 $\times2$, 6×2, and c(12×2) models with vertical reconstruction. Unfortunately, after relaxations, we found that the Ag atoms were restored back to their original heights at the β_T and β_T' sites. This seem to suggest that the multiwell potential along the z axis is unlikely.[18] We note that Miyata *et al.*[18] also proposed two other explanations for the double periodicity which can be either due to pairing up of neighboring Ag atoms or through lateral zigzag shifts of Ag atoms, aside from the out-of-plane fluctuations of Ag atoms. However, they concluded that these out-of-plane fluctuations look more plausible than the two in-plane fluctuations.

IV. CONCLUSIONS

The atomic and electronic structures of the c(12×2) phase in Ag-induced Si(111) reconstructions at Ag coverage of 1/3 ML have been investigated by means of first-principles calculations. The mechanisms of phase transitions from 3×1 to 6×1 and from 6×1 to c(12×2) have also been examined. Our calculations confirm that the c(12×2) and 6×1 models are all derived from the HCC 3×1 model. The phase transition from 3×1 to 6×1 results from the collective movement of atoms such that the Ag atoms in the adjacent row are located in the two equivalent sites (β_T and β_T'). By contrast, the phase transition from 6×1 to c(12 $\times2$) can be attributed to the dimerization of Ag atoms in the Ag rows in the 6×1 phase. Moreover, the identified c(12 $\times2$) model in this study has a lower energy than the 6×1 and 3×1 phases. The energy ordering of 3×1, 6×1, and c(12×2) models is consistent with the conception of a sequence of two order-disorder transitions. Finally, the simulated STM images of this c(12×2) model are in excellent agreement with the experimental STM images.

ACKNOWLEDGMENTS

F.C.C. acknowledges support from NCST and National Science Council of Taiwan under Grant No. NSC95-2112-M110-022-MY3. We are grateful to the National Center for High-performance Computing for computer time and facilities. C.Z.W. and K.M.H. acknowledge support from the Director of Energy Research, Office of Basic Energy Sciences, which includes a grant of computer time at the National Energy Research Supercomputing Center (NERSC) in Berkeley. Ames Laboratory was operated for the U.S. Department of Energy by Iowa State University under Contract No. DE-AC02-07CH11358.

*fchuang@mail.nsysu.edu.tw

[1] V. Barone, G. Del Re, G. Le Lay, and R. Kern, Surf. Sci. **99**, 223 (1980).
[2] M. Saitoh, F. Shoji, K. Oura, and T. Hanawa, Surf. Sci. **112**, 306 (1981).
[3] G. Le Lay, A. Chauvet, M. Manneville, and R. Kern, Appl. Surf. Sci. **9**, 190 (1981).
[4] T. Yokotsuka, S. Kono, S. Suzuki, and T. Sagawa, Surf. Sci. **127**, 35 (1983).
[5] G. Le Lay, Surf. Sci. **132**, 169 (1983).
[6] R. J. Wilson and S. Chiang, Phys. Rev. Lett. **58**, 369 (1987).
[7] W. C. Fan and A. Ignatiev, Phys. Rev. B **41**, 3592 (1990).
[8] K. J. Wan, X. F. Lin, and J. Nogami, Phys. Rev. B **46**, 13635 (1992); **47**, 13700 (1993).
[9] T. Fukuda, Phys. Rev. B **50**, 1969 (1994).
[10] J. M. Carpinelli and H. H. Weitering, Surf. Sci. **331–333**, 1015 (1995).
[11] S. C. Erwin, Phys. Rev. Lett. **75**, 1973 (1995).

[12] L. Lottermoser, E. Landemark, D.-M. Smilgies, and M. Nielsen, R. Feidenhans'l, G. Falkenberg, R. L. Johnson, M. Gierer, A. P. Seitsonen, H. Kleine, H. Bludau, H. Over, S. K. Kim, and F. Jona, Phys. Rev. Lett. **80**, 3980 (1998).
[13] C. Collazo-Davila, D. Grozea, and L. D. Marks, Phys. Rev. Lett. **80**, 1678 (1998).
[14] S. C. Erwin and Hanno H. Weitering, Phys. Rev. Lett. **81**, 2296 (1998).
[15] G. Le Lay, J. M. Layet, A. Cricenti, C. Ottaviani, and P. Perfetti, Surf. Sci. **438**, 97 (1999).
[16] M. Gurnett, J. B. Gustafsson, K. O. Magnusson, S. M. Widstrand, and L. S. O. Johansson, Phys. Rev. B **66**, 161101(R) (2002).
[17] Kazuyuki Sakamoto, Hidenori Ashima, H. M. Zhang, and Roger I. G. Uhrberg, Phys. Rev. B **65**, 045305 (2001); Kazuyuki Sakamoto and R. I. G. Uhrberg, e-J. Surf. Sci. Nanotechnol. **2**, 210 (2004).
[18] N. Miyata and I. Matsuda, M. D'angelo, H. Morikawa, T. Hirahara, and S. Hasegawa, e-J. Surf. Sci. Nanotechnol. **3**, 151 (2005).
[19] T. Furuhashi, Yoshifumi Oshima, and Hiroyuki Hirayama, Appl. Surf. Sci. **253**, 651 (2006).
[20] K. Sumitani, K. Masuzawa, T. Hoshino, R. Yoshida, S. Nakatani, T. Takahashi, H. Tajiri, K. Akimoto, H. Sugiyama, X.-W. Zhang, and H. Kawata, Surf. Sci. **601**, 5195 (2007).
[21] S. C. Erwin, Phys. Rev. Lett. **91**, 206101 (2003); C. Battaglia, Philipp Aebi, and S. C. Erwin, Phys. Rev. B **78**, 075409 (2008).
[22] S. Riikonen and D. Sánchez-Portal, Phys. Rev. B **71**, 235423 (2005).
[23] C.-Y. Ren, S.-F. Tsay, and F.-C. Chuang, Phys. Rev. B **76**, 075414 (2007).
[24] Feng-Chuan Chuang, Chia-Hsiu Hsu, Cai-Zhuang Wang, and Kai-Ming Ho, Phys. Rev. B **77**, 153409 (2008).
[25] C. Z. Wang, B. C. Pan, and K. M. Ho, J. Phys.: Condens. Matter **11**, 2043 (1999).
[26] F. C. Chuang, Ph.D. thesis, Iowa State University, Ames, IA USA, 2005.
[27] J. P. Perdew, K. Burke, and M. Ernzerhof, Phys. Rev. Lett. **77**, 3865 (1996).
[28] P. Hohenberg and W. Kohn, Phys. Rev. **136**, B864 (1964); W. Kohn and L. J. Sham, *ibid.* **140**, A1133 (1965).
[29] G. Kresse and D. Joubert, Phys. Rev. B **59**, 1758 (1999).
[30] G. Kresse and J. Hafner, Phys. Rev. B **47**, 558 (1993); G. Kresse and J. Furthmuller, *ibid.* **54**, 11169 (1996).
[31] There are 4845 ($C_4^{20}=\frac{20!}{4!\times 16!}=4845$) and 7315 ($C_4^{22}=\frac{22!}{4!\times 18!}=7315$) models for the HCC-like and DHC-like (6×2) cells, respectively. Taking translational symmetry further into account and excluding 45 and 55 (6×1) models, only 2400 and 3630 models are unique. ($\frac{4845-55}{2}=2400$ and $\frac{7315-55}{2}=3630$).
[32] J. Tersoff and D. R. Hamann, Phys. Rev. B **31**, 805 (1985).